Immune modulation and monitoring of cell therapy in inflammatory disorders

Suwandi, J.S.

Chapter 4.2

Multidimensional analyses of proinsulin peptide-specific regulatory T cells induced by tolerogenic dendritic cells

Jessica S. Suwandi*, Sandra Laban*, Kincsö Vass, Antoinette Joosten, Vincent van Unen, Boudewijn P.F. Lelieveldt, Thomas Höllt, Jaap Jan Zwaginga, Tatjana Nikolic* and Bart O. Roep*

*Contributed equally.

Journal of Autoimmunity 2019, 107, 102361

Abstract

Induction of antigen-specific regulatory T cells (Tregs) *in vivo* is the holy grail of current immune-regulating therapies in autoimmune diseases, such as type 1 diabetes. Tolerogenic dendritic cells (tolDCs) generated from monocytes by a combined treatment with vitamin D and dexamethasone (marked by $CD52^{hi}$ and $CD86^{lo}$ expression) induce antigen-specific Tregs. We evaluated the phenotypes of these Tregs using high-dimensional mass cytometry to identify a surface-based T cell signature of tolerogenic modulation. Naïve $CD4^+$ T cells were stimulated with tolDCs or mature inflammatory DCs pulsed with proinsulin peptide, after which the suppressive capacity, cytokine production and phenotype of stimulated T cells were analysed. TolDCs induced suppressive T cell lines that were dominated by a naïve phenotype ($CD45RA^+CCR7^+$). These naïve T cells, however, did not show suppressive capacity, but were arrested in their naïve status. T cell cultures stimulated by tolDC further contained memory-like ($CD45RA^-CCR7^-$) T cells expressing regulatory markers Lag-3, CD161 and ICOS. T cells expressing $CD25^{lo}$ or $CD25^{hi}$ were most prominent and suppressed $CD4^+$ proliferation, while $CD25^{hi}$ Tregs also effectively supressed effector $CD8^+$ T cells.

We conclude that tolDCs induce antigen-specific Tregs with various phenotypes. This extends our earlier findings pointing to a functionally diverse pool of antigen-induced and specific Tregs and provides the basis for immune-monitoring in clinical trials with tolDC.

Keywords: Regulatory T cells, Tolerogenic Dendritic Cells, Immune Therapy, Mass Cytometry

Introduction

T regulatory cells (Tregs) are specialized to control auto-immune responses and therefore vital in maintaining immune homeostasis. In type 1 diabetes, however, loss of tolerance to β-cell antigens results in the destruction of insulin-producing cells. Strategies to induce or increase Tregs have been developed in an effort to reduce immune inflammation in patients with autoimmune diseases (1-5). In an attempt to induce islet antigen-specific Tregs, we established that dendritic cells (DCs) treated with $1,25(OH)_2$ vitamin D3 (1,25-dihydroxycholecalciferol; VitD3) and dexamethasone (VitD3/Dex) during their modulation and maturation from monocytes induce antigen-specific Tregs *in vitro* (6-9). These tolerogenic DCs (tolDC) additionally show various suitable functional traits such as islet autoantigen-dependent inhibition of effector T cells (6), elimination of cytotoxic $CD8^+$ T cells (10, 11) and homing characteristics to the disease lesion (8, 12). Moreover, the effect of tolDC was demonstrated *in vivo* using a humanized transgenic mouse model, where proinsulin peptide-pulsed tolDCs prevented and reversed autoimmunity to proinsulin (13). Therapy with tolDCs loaded with specific antigens therefore appears a promising approach to reduce autoimmunity and introduce antigen-specific tolerance in type 1 diabetes. The safety of this strategy has been tested recently in a phase I clinical trial (https://www.trialregister.nl/trial/5425).

One of the major challenges encountered in immunomodulating trials is the lack of specific surface markers to determine the induction of adaptive immune tolerance, including induction or expansion of adaptive Tregs *in vivo*. Naturally occurring Tregs (nTregs) show consistent expression of the intracellular transcription factor Foxp3 that is often used as a Treg specification marker (14). Although the role of Foxp3 as biomarker of tolerance is evident (15, 16), both adaptive Tregs, e.g. Tr1 cells (17, 18), show low or transient expression of Foxp3 similar to activated effector T cells (19, 20). In contrast, other surface molecules such as Lag-3, CTLA-4, PD-1, ICOS, CCR4, CD39, HLA-DR are present on subsets of nTreg (21) as well as on adaptive Tregs (8, 22) and

may be more useful for detection of induced suppressive T cells. Moreover, our previous data on tolDC-induced Tregs pointed to a diversity of Treg subtypes at a clonal level based on the intracellular cytokines and suppressive mechanisms (22). Further determining the cell surface maker signatures of tolDC-induced Tregs may provide means for monitoring Treg induction in human trials.

In this study, we applied mass cytometry (CyTOF) detecting 35 surface markers simultaneously. The innovative Cytosplore software (23) enabled analyses of this high-dimensional data set with single-cell resolution using Hierarchical Stochastic Neighbor Embedding (HSNE) (23-25). This novel approach enabled us to extend previous studies with current in-depth investigation of surface marker expression patterns of pro-insulin specific Tregs induced by tolDCs and to correlate to their capacity to suppress T cell proliferation.

Material and methods

Generation and quality control of human tolDCs and mDCs

Human peripheral blood mononuclear cells (PBMC) were isolated with Ficoll density gradient centrifugation from HLA-typed buffy coats purchased from Sanquin. All participants have given a written informed consent. The protocol of generating monocyte derived mDCs and tolDCs has been described (6). After 48 hours of activation with LPS (100 ng/mL) and human GM-CSF (800 U/mL), matured tolDCs and mDCs were stained for FACS analysis. Cells were washed with FACS buffer (PBS/0,5%BSA/0,02%Azide) and stained with APC-labelled PD-L1 (clone MIH1, Ebioscience, Cat# 17-5983-42, Lot# E12159-1634) and CD25 (clone M-A251, BD, Cat# 560987, Lot# 5176736), FITC-labelled CD52 (clone YTH34.5, Serotec AbD, Cat# MCA1642F, Lot# 0215) and PE-labelled CD86 (clone 2331, BD, Cat# 560957, Lot# 5128592). Flow cytometric staining was analysed on the FACS Canto II (BD) and data analysis was performed using FlowJo V10.

Inducing T_{tolDC} and T_{mDC} lines from naïve CD4$^+$ T cells

Cryopreserved immature tolDCs and control DCs were thawed and activated for 48 hours with LPS (100 ng/mL, Sigma-Aldrich Chemie) in the presence of human GM-CSF (800 U/mL, Invitrogen). Naïve autologous CD4$^+$ T cells were isolated from CD14 negative fraction using untouched human CD4$^+$ T cell kit (Dynal, Invitrogen) or naïve CD4$^+$ T cell isolation kit (MACS, Miltenyi Biotec), according to the suppliers' protocol. To exclude the possibility that suppressive T cells expand or arise from activated nTregs, CD25^{hi} T cells were depleted in the isolation method of naïve CD4$^+$ T cells. Activated tolDCs or mDCs were loaded with pro-insulin peptide C19A3 for 4 hours (7.5 ug/ml) and co-cultured with naïve CD4$^+$ T cells to induce antigen specific T cell lines (T_{tolDC} and T_{mDC} respectively) as described previously (9).

Flow cytometry-based sorting of T cells

T_{tolDC} and T_{mDC} lines were activated for 24 hours with mDCs pulsed with C19A3 peptide as previously described and stained for sorting. Staining was performed on ice. Cells were washed with PBS/2%FCS and stained with APC-Cy7-labelled CD25 (clone M-A251, BD, Cat# 557753, Lot# 64916) and AF700-labelled CD45RA (clone HI100, Biolegend, Cat# 555365, Lot# B227350) for 30 minutes. Thereafter, cells were washed twice and taken up in PBS/2%FCS. Finally, sorting was done on FACSAria III (BD) and cells were collected in 50% FCS and 50% IMDM.

Suppression of allogeneic naïve $CD4^+$ T cells

To assess capacity of T_{tolDC} and T_{mDC} lines to suppress proliferation of naïve $CD4^+$ T cells, allogeneic donors (donor A) were selected to mismatch with the DC and T cell donors (donor B) bearing HLA-DR4 (the HLA restriction element of the proinsulin peptide C19-A3), to allow quantification of antigen-specific suppression. Naïve $CD4^+$ T cells from donor A were labelled with 0,5 µM/ml CFSE (per $2*10^6$ cells/ml) and cultured in the presence of activated and C19A3 loaded mDCs from donor B at a 10:1 ratio in a 96 round bottom plate, coated with 0,1 µg/ml anti-human CD3 mAb (clone UCHT1, BD). Purified naïve T cells (control for crowding), T_{tolDC} or T_{mDC} cells from donor B were added at a 1:1 ratio to the CFSE labelled responder T cells. Each condition was tested in triplicate. After 4 days, cells were recovered and analysed on the FACS Calibur (BD). Prior to the analysis, 10,000 Flow-Count Fluorospheres were added (Beckman Coulter). For each sample, 5000 fluorosphere events were acquired for quantitative comparison of samples. Division (d) of responder cells were calculated as expansion index (EI) using de formula (n=number of divisions):

$$\int_{d=0}^{d=n} EI\ (d) = \frac{\sum Events(d)}{\sum Events(d)/2^n}$$

An expansion index of 1.0 (no division) forms the 0% proliferation value. Proliferation of CFSE labelled naïve $CD4^+$ T cells in the presence of naïve $CD4^+$ T cells (crowding control) forms the 100% proliferation value.

Suppression of cytotoxic CD8⁺ T cells

To assess whether T_{tolDC} and T_{mDC} lines suppress cytotoxic CD8⁺ T cells, a cytotoxicity assay was performed using B cell line (JY) as target cells and clonal PPI-specific CD8⁺ T cells as effector(10). Target B cells were labelled with a high dose of CFSE (1 µM/ml), representing a bystander target ($CFSE^{high}$) or labelled with a low dose of CFSE (0,1 µM/ml) and pulsed PPI peptide (5 ug/ml) to serve as a specific target ($CFSE^{low+PPI}$) of PPI-specific CD8⁺ T cells. $CFSE^{low+PPI}$ and $CFSE^{high}$ target cells were co-cultured overnight with sorted T_{tolDC} in 1:1:2 ratio. During the last 4 hours, PPI-specific CD8⁺ T cells were added in 1:1 and 1:5 (specific target : effector) ratio, after which cells were recovered and analysed on the FACS Calibur (BD). Each condition was tested in duplicate. Percentage killing was calculated by using the formula:

$$Lysis = L(x) = \frac{(a-b)}{a+b}$$

a = $CFSE^{high}$ target cell

b = $CFSE^{low+PPI}$ target cell

$$\%\ Inhibition = 100 - \frac{L(T_{tolDC}) - L(no\ CD8)}{L(no\ T_{tolDC}) - L(no\ CD8)} * 100\%$$

Specific lysis was calculated by normalizing for spontaneous cell death in the absence of PPI-specific CD8⁺ T cells. Inhibition of specific lysis was calculated by dividing specific killing in the presence of a T_{tolDC} line or a sorted cell subset with specific killing with PPI-specific CD8⁺ T cells added alone (100% lysis).

Intracellular Foxp3 staining

T_{tolDC} were stimulated overnight with C19A3-pulsed mDC and washed with FACS buffer. Cells were fixed and thereafter stained with AF647-labelled Foxp3 (clone 259D, Beckman Coulter, Cat# B30650) in permeabilizing reagent (PerFix-nc Kit, Beckman Coulter) for 1 hour at room temperature. Fluorescent staining was measured on the FACS Calibur (BD).

Cytokine release assays

T_{tolDC} and T_{mDC} cells were stimulated for 24 hours with activated mDCs loaded with C19A3 peptide at a 10:1 ratio in a 96 round bottom plate. Supernatant was taken and stored at -80°C until analysis. Cytokine analysis was done with Luminex 9-plex kit of BioRad according to the manufacturer's protocol.

Staining T_{tolDC} and T_{mDC} lines for CyTOF and data acquisition

The CyTOF antibody staining panel consisted of 35 surface markers including markers described for Tregs, lineage, differentiation and activation (Table 1). Metal-conjugated antibodies were either purchased or conjugated as described previously (26). T_{tolDC} and T_{mDC} lines were activated for 24 hours with mDCs pulsed with C19A3 peptide and stained for CyTOF analysis. For this, cryopreserved T_{tolDC} and T_{mDC} lines were thawed, washed and stimulated overnight with C19A3 peptide loaded mDC at a 10:1 ratio in a 96 round bottom plate. Staining was performed the next day, as previously described (26).

Analysis of CyTOF data

Live and single cells were distinguished using DNA stains and event length in FlowJo V10. Beads were excluded and cells were gated to be $CD4^+$, $CD45^+$, $TCRgd^-$ and $CD8^-$ and used for further analysis. PCA analysis of samples was performed using Partek software, version 7.0 2018 (Partek Inc., St. Louis, MO, USA). Next, SPADE trees were generated in Cytobank (27) with 200 target number nodes and 10% down sampled event target. Finally, dimensionality reduction technique HSNE implemented in Cytosplore (25) (version 2.2.0) was used for in-depth analysis of the dataset without down sampling. The amount of hierarchical levels suitable for HSNE analysis was determined with the formula $\log_{10}(n/100)$ and was set to 4 (n=1,016,321 cells). Values were Arcsine transformed and HSNE analysis was performed based on the expression of the 35 markers listed in table 1. Using the Gaussian-mean-shift method subsequent clusters were generated. Heatmaps were generated using R software (R package,

version 99.902). Packages 'flowcore', 'ggplot2', 'gplots' and 'heatmap.2' were used to assist in clustering and heatmap drawing.

Statistics

Statistical analysis was performed with GraphPad Prism version 7.00 (GraphPad Software, La Jolla California, USA). To compare differences in suppression and fold-expansion between T_{tolDC} and T_{mDC} lines, data were compared by a two-sided Student's t-test (paired). One-way ANOVA followed by Dunnett's multiple comparisons test was used to compare the suppression of sorted T cell populations. Cytokine production of T_{tolDC} and T_{mDC} lines was compared using Wilcoxon matched-pairs signed-rank test, statistical significance was corrected for multiple comparisons with the Benjamini and Hochberg procedure. Median expression values were normalized by log10 transformation and subsequently analysed using multiple t-tests, statistical significance was corrected for multiple comparisons using the Holm-Sidak method.

Table 1. Staining panel for mass cytometry

Marker	Metal	Clone	Dilution
CD3	170Er	UCHT1	1:100
CD4	145Nd	RPA-T4	1:200
CD7	153Eu	CD7-6B7	1:100
CD8a	146Nd	RPA-T8	1:50
CD16	148Nd	3G8	1:100
CD20*	163Dy	2H7	1:200
CD25	149Sm	2A3	1:100
CD27	167Er	O323	1:100
CD28*	171Yb	CD28.2	1:100
CD38	172Yb	HIT2	1:200
CD39*	162Dy	A1	1:100
CD45	89Y	HI30	1:100
CD45RA	169Tm	HI100	1:100
CD45RO*	173Yb	UCHL1	1:100
CD49b*	176Yb	P1e6c5	1:100
CD69	144Nd	FN50	1:50
CD103*	155Gd	Ber-ACT8	1:50
CD107 (LAMP)*	143Nd	H4A3	1:50
CD122*	158Gd	TU27	1:50
CD126 (IL6R)*	154Sm	UV4	1:40
CD127	165Ho	AO19D5	1:200
CD152 (CTLA4)*	166Er	14D3	1:40
CD161	164Dy	HP-3G10	1:100
CD194 (CCR4)	156Gd	L291H4	1:100
CD196 (CCR6)	141Pr	G034E3	1:100
CD197 (CCR7)	159Tb	G043H7	1:100
CD223 (Lag-3)	150Nd	874501	1:40
CD278 (ICOS)	151Eu	DX29	1:50
CD279 (PD-1)	175Lu	EH 12.2H7	1:100
CD335 (NKp46)*	174Yb	9E2	1:50
CD336 (Nkp44)*	147Sm	P44-8	1:50
CD357 (GITR)*	142Nd	621	1:40
HLA-DR*	168Er	L243	1:200
KLRG-1*	160Gd	REA261	1:50
TCRgd	152Sm	11F2	1:50

*self-conjugated

Results

TolDCs expressing low CD86 induce suppressive T cell lines

Naïve $CD4^+$ T cells were stimulated by proinsulin peptide C19A3-loaded autologous tolDC or matured inflammatory DCs (mDC) (the generated T cell cultures further referred to as T_{tolDC} and T_{mDC}, respectively). After two rounds of antigen-specific stimulation, T_{tolDC} and T_{mDC} cells were tested in a suppression assay using a previously established protocol (6, 8, 9, 22, 28). In short, proliferation of allogeneic CFSE labelled naïve $CD4^+$ T cells in the presence of T_{tolDC} or T_{mDC} and C19A3-pulsed mDC (10:10:1 ratio T_{CFSE}: T_{tolDC}/T_{mDC}: DC) was measured after 4 days of co-culturing. The proliferation of CFSE-labelled responder T cells was suppressed in the presence of T_{tolDC} cells whereas enhanced in the presence of T_{mDC} cells, compared to the proliferation in the presence of purified naïve T cells as crowding control (paired t-test; p=0.04; Figure 1A). Two out of eight T_{tolDC} lines showed no suppressive activity (Figure 1A), which was associated with the inability to induce tolDCs expressing low levels of CD86 (Figure 1D). This is in line with our previous report where low CD86 expression was important to characterize tolerogenic modulation of DCs (6, 29). Indeed, other characteristics of these two non-suppressive T_{tolDC} lines were also discordant with suppressive $T_{tolDC.}$ In the suppressive T_{tolDC} lines, the yield was similar to the number of naïve T cells at the start of culture, whereas the cell number in the two non-suppressive T_{tolDC} lines increased 3 and 8-fold compared to the start (Figure 1B). The yield of T cells stimulated by mDCs was on average 12-fold higher after culture (paired t-test; p=0.003) (Figure 1B). The production of IL-5, IL-10, IL-13, IFN-g and TNF-a was evaluated after re-stimulation with C19A3-pulsed mDCs. Suppressive T_{tolDC} lines produced significantly lower amounts of IL-5, IL-10, IL-13 and TNFa as compared to their T_{mDC} counterparts (Wilcoxon signed-rank test; p=0.019 for all cytokines; Figure 1C), whereas this trend was not observed in non-suppressive T_{tolDC} lines. Altogether, T cells stimulated with tolDCs or mDCs showed a dichotomy in suppressive capacity and cytokine production, while tolDCs expressing high CD86 induced non-suppressive T cells similar to mDC stimulated cultures.

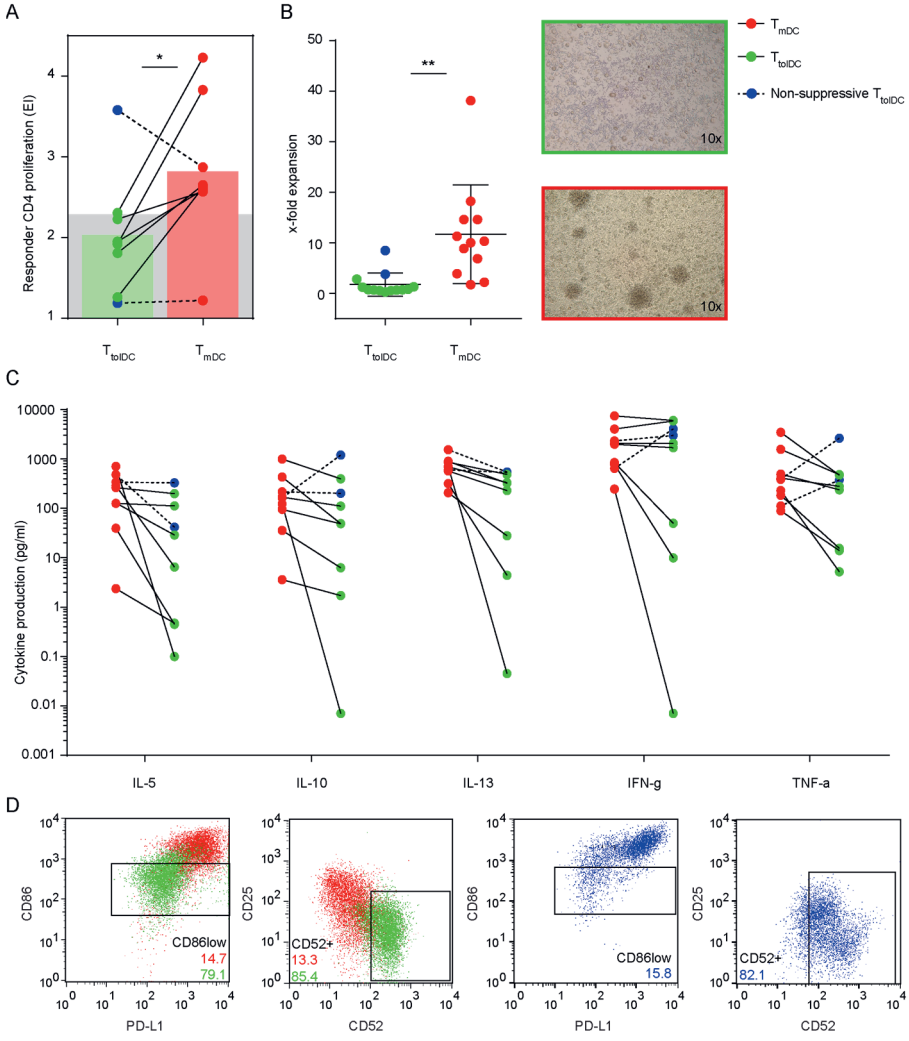

Figure 1. TolDC phenotype correlates with the capacity to induce suppressive T cells. A) The suppressive capacity of T_{tolDC} and T_{mDC}. mDCs pulsed with C19A3 were co-cultured with CFSE-labelled allogeneic naïve $CD4^+$ T cells in the presence of T_{tolDC} or T_{mDC} (ratio 1:10:10). Proliferation was calculated based on the expansion index (EI) and the grey bar depicts the proliferation in presence of naïve $CD4^+$ T cells (crowding control). T_{tolDC} inhibited the proliferation of naïve $CD4^+$ T cells, whereas T_{mDC} stimulated the proliferation of naïve $CD4^+$ T cells, n=8 per group (paired t-test; p=0.045). Two T_{tolDC} lines (blue symbols) did not suppress proliferation of responder $CD4^+$ T cells, compared to the autologous T_{mDC} line. B) Fold expansion of T cells in culture. T cells stimulated with mDC expanded on average 12-fold, whereas tolDC -stimulated T cells did not increase in number after two weeks co-culture, n=12 per group (paired t-test p=0.003). The two non-suppressive T_{tolDC} lines did expand 3-fold and 8- fold in culture. Picture inserts show T cells after 5 days of co-culture with tolDC (green frame) or mDC (red frame). C) Cytokine production by T_{tolDC} and T_{mDC} during overnight stimulation with proinsulin peptide-pulsed mDC. T_{mDC} lines produced significantly more IL-5, IL-

10, IL-13 and TNF-a than suppressive T_{tolDC} lines, n=7 per group (Wilcoxon signed rank test; p=0,019 for all four cytokines). Non-suppressive T_{tolDC} were not included in the statistical analysis. D) Left panel shows representative phenotype of tolDCs (green) and mDCs (red) used to stimulate T cells determined by CD86 and CD52 expression. Right panel shows the phenotype of tolDCs used to induce the non-suppressive T_{tolDC} line (blue).

High-dimensional phenotype analysis of T_{tolDC} and T_{mDC} lines with mass cytometry

To extensively characterize the surface phenotype of the suppressive T cells induced by tolDCs, we employed CyTOF technology to analyse five independently generated T_{tolDC} lines and corresponding T_{mDC} lines, of which one was a non-suppressive T_{tolDC} line. The median expression of the 35 tested surface molecules was evaluated, revealing differential expression patterns between T_{tolDC} and T_{mDC} lines (Figure 2A). T_{tolDC} lines showed higher expression of CD27 and CD45RA than T_{mDC} (multiple t-tests; p=0.049 and p<0.0001, respectively). The expression of CCR4, CD45RO, CD39, CD38 and CD25 was lower in T_{tolDC} than in T_{mDC} lines (multiple t-tests; p=0.049, p=0.03, p<0.0001, p=0.009 and p=0.01, respectively). The phenotype of the non-suppressive T_{tolDC} line differed from the suppressive T_{tolDC} lines, as well as from T_{mDC} lines. We further performed principal component analysis (PCA) to cluster the generated T cell lines, integrating the median expression patterns of all markers simultaneously (Figure 2B). The T_{tolDC} and T_{mDC} lines clustered separately, while the non-suppressive T_{tolDC} line clustered within the T_{mDC} lines. These results demonstrate differences in surface phenotypes of T cell lines induced by tolDCs versus mDCs.

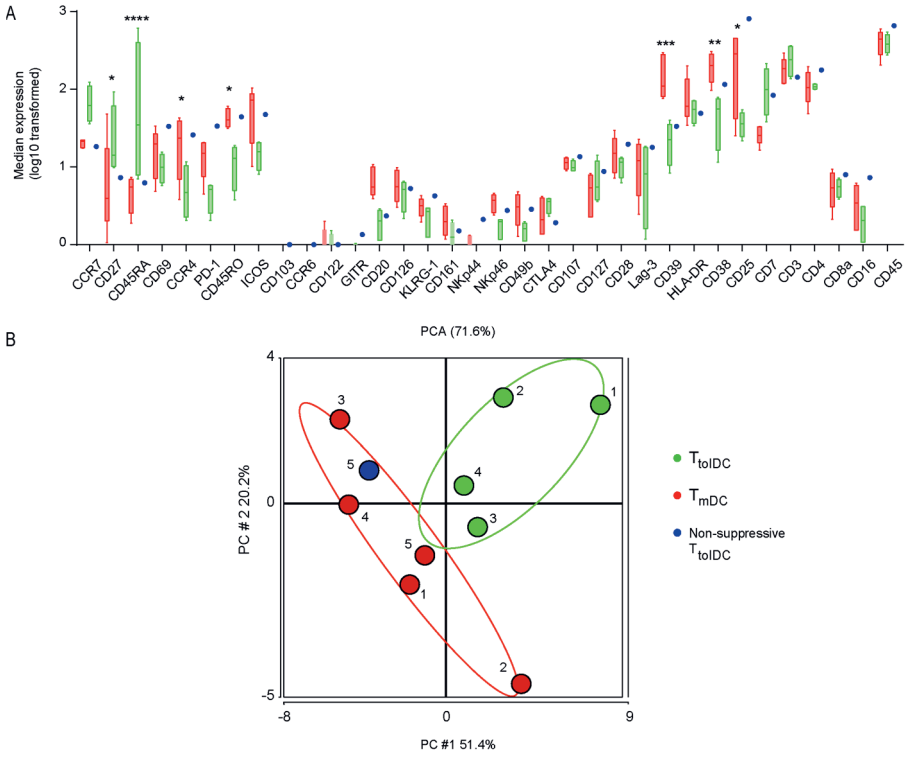

Figure 2. T_{tolDC} and T_{mDC} lines show distinct phenotypes. T cell lines were stimulated overnight with proinsulin-pulsed mDC and labelled with a CyTOF antibody panel. The green symbols depict suppressive T_{tolDC}, red symbols depict T_{mDC} and blue symbol shows the phenotype of the non-suppressive T_{tolDC} line. A) Log10 transformed median expression of T_{tolDC} and T_{mDC}, the whiskers visualise the range minimum to maximum. The lines show different expression of CD27, CD45RA, CCR4, CD45RO, CD39, CD38 and CD25, T_{tolDC} n=4 and T_{mDC} n=5 (multiple t-tests; p=0.049, p<0.0001, p=0.049, p=0.025, p<0.0001, p=0.009 and p=0.01). The non-suppressive T_{tolDC} was not included in the statistical analysis. B) Principal Component Analysis of T_{tolDC} and T_{mDC} lines based on the median expression of 35 immune markers. The non-suppressive T_{tolDC} line included in the analyses, clusters close to the T_{mDC} lines and separately from the suppressive T_{tolDC} lines.

Next, we analysed the T_{tolDC} and T_{mDC} lines using the SPADE algorithm (30) and visualised these individually to explore the variability between and within T_{tolDC} and T_{mDC} lines. In the SPADE analysis, the multidimensional data set is down sampled and clustered into a two-dimensional tree such that cells with a similar phenotype cluster into a node, where the node branch is based on the differences in the marker expression pattern between clusters (Figure 3). Overall, T_{tolDC} lines showed different cluster distributions compared to T_{mDC} lines, although variation in cluster size was

detectable within the T_{tolDC} or T_{mDC} lines. Moreover, the non-suppressive T_{tolDC} line lacked a group of clusters that were present in the other suppressive T_{tolDC} lines (Figure 3, grey arrow). To evaluate the phenotype of these clusters, we visualised the marker expressions as a colour overlay (Supplementary Figure 1). Clusters specific to the suppressive T_{tolDC} lines only were $CD45RA^{+}CCR7^{+}CD25^{lo}$. Other three SPADE branches represented distinct clusters of T cells expressing CD25 and CCR6, co-expressing Lag-3, CTLA4 and GITR and were present in both the T_{tolDC} and T_{mDC} lines.

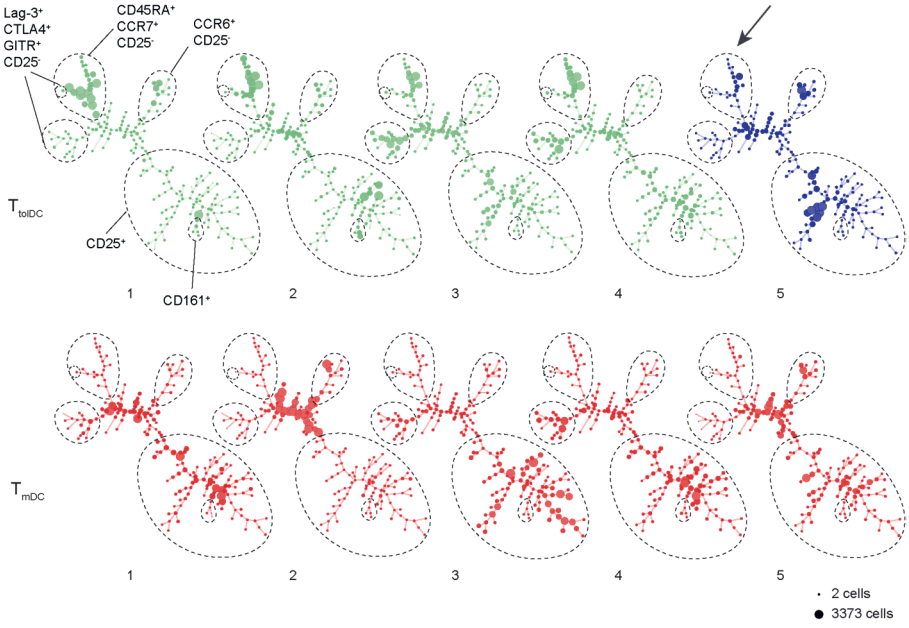

Figure 3. Multidimensional SPADE analysis of T_{tolDC} and T_{mDC} lines. T_{tolDC} lines (green) show differential cluster distribution in the SPADE analysis from the T_{mDC} lines (red). The non-suppressive T_{tolDC} line (blue) shows different distribution than the suppressive T_{tolDC} lines. Circles depict clusters with designated marker expression as shown in Supplementary Figure 1. The grey arrow indicates the clusters lacking in the non-suppressive T_{tolDC} line.

To further dissect the composition of the T_{tolDC} and T_{mDC} lines, a Hierarchical Stochastic Neighbor Embedding (HSNE) analysis was performed. This novel dimensionality reduction technique implemented in the Cytosplore platform (23-25), enabled the analysis of our large data consisting of 1,016,321 cells without having to down sample data by constructing a hierarchy which can be explored stepwise up to the single-cell

level. This strategy allows the efficient detection of low frequent cell subsets (25). A global view of data derived from the T_{tolDC} and T_{mDC} lines is visualised in Figure 4A. Three main groups were formed using the Gaussian-mean-shift method and each group was further inspected by zooming into the single-cell data level (Figure 4B). The three main groups were distinguished by the expression of CD45RA, CCR7 and CD25; group A largely consisted of cells expressing CD45RA, CCR7 and low levels of CD25, group B of cells negative for CD45RA and low expression of CCR7 and CD25, and group C of cells lacking CD45RA and CCR7 but expressing high levels of CD25. Further clustering of these groups resulted in seven smaller clusters within group A; seven clusters in group B and six clusters in group C. The phenotypes of the generated clusters were visualised in a heatmap (Figure 4C) together with the number of cells per cluster originating from the suppressive T_{tolDC} line, non-suppressive T_{tolDC} lines and T_{mDC} lines (Figure 4C and Supplementary Table 1). The clusters in group A contained T cells with a naïve phenotype (clusters A3-A7) and consisted mainly of suppressive T_{tolDC} cells, matching the SPADE analysis. This group was further characterized by the high expression of CD7 and CD27. Cell clusters A1 and A2 were distinct from the general phenotype of group A, exemplified by the lack of CCR7 expression, demarcating a T_{EMRA} phenotype, of which one cluster (A1) specifically expressed CD161. The clusters in group B displayed an effector memory (EM; $CD45RA^{-}CCR7^{-}CD25^{hi}$) phenotype, while group C displayed a central memory (CM; $CD45RA^{-}CCR7^{lo}CD25^{lo}$) phenotype, consisting of cells derived from both the T_{tolDC} and the T_{mDC} lines. However, T_{mDC} lines contained more EM cells than T_{tolDC} lines, and these co-expressed HLA-DR, CD39, CD38 CD69, ICOS, CD45RO, CD28, PD-1 and CCR4. The clusters with a CM phenotype were also more abundant in T_{mDC} lines, with the exception of two clusters (C4 and C5) co-expressing Lag-3 CTLA4 and GITR, which largely contained T_{tolDC}-originating cells. The signatures of T_{tolDC} and T_{mDC} lines analysed separately in HSNE (Supplementary Figure 2), confirmed the presence of the specific clusters in T_{tolDC} or T_{mDC} lines.

In summary, using three independent methods to analyse the phenotype of T_{tolDC} and T_{mDC} cells, we show that T cell lines stimulated with tolDCs acquire substantially different phenotypes than T cells stimulated with mDCs. The abundant presence of $CD45RA^{+}CCR7^{+}CD25^{lo}$ naïve T cells marked suppressive T_{tolDC} lines, while cells with CM and EM phenotypes were abundant in both T_{mDC} and T_{tolDC} lines. Two T_{EMRA}-like and two CM subsets were enriched in the suppressive T_{tolDC} lines.

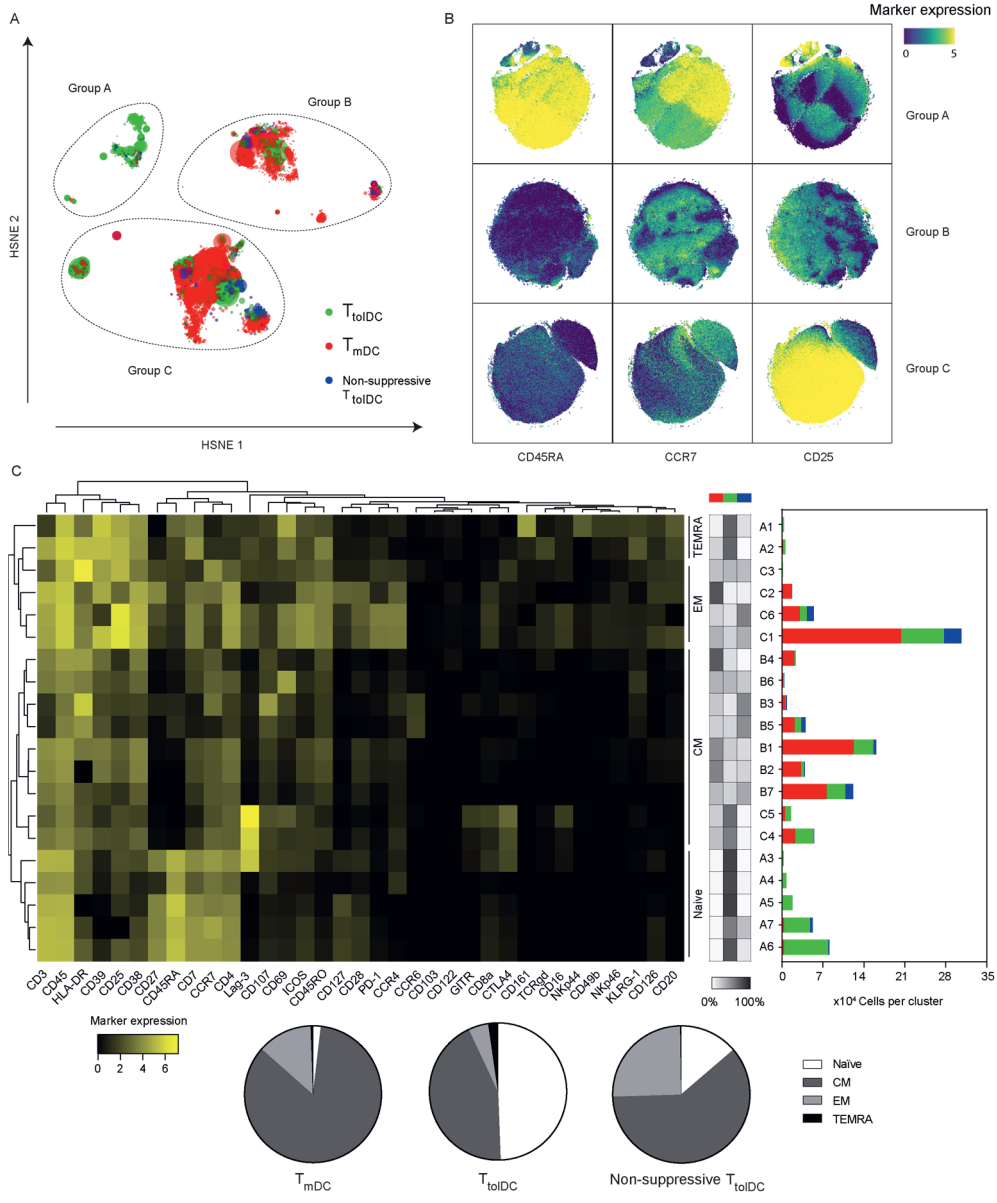

Figure 4. High dimensional analysis comparing T_{tolDC} and T_{mDC} lines. The CyTOF data of T_{tolDC} and T_{mDC} were analysed together using Hierarchical Stochastic Neighbor Embedding (HSNE). HSNE integrates the information of 35 markers measured on a single cell level in a two-dimensional HSNE map. A) Groups A, B and C depict three major landmarks in the HSNE overview level. Green areas depict cells originating from T_{tolDC}, blue areas: cells from the non-suppressive T_{tolDC} line, red areas: cells from T_{mDC} lines. B) tSNE plots of landmark groups A, B and C were visualised (at single-cell data level) with respect to expression of CD45RA, CCR7 and CD25. Group A consists mainly of $CD45RA^{+}$ cells, group B consists of $CD45RA^{-}$ and $CD25^{lo}$ cells

and CD25^{hi} cells were mainly found in group C. C) Heatmap of the HSNE. Resulting clusters are visualised as rows in the heatmap. Cluster names refer to the originating group. Heatmap in the middle panel visualises the distribution relative to the number of cells in a cluster. The right histogram shows the abundance of cells within the cluster in absolute numbers, taking into account the origin of cells (green: T_{tolDC}, blue: non-suppressive T_{tolDC} line, red: T_{mDC}). Statistics of the histogram are shown in Supplementary Table 1. The three pie-charts depict the percentage of cells with a naïve, CM, EM or TEMRA phenotype within the T_{mDC}, T_{tolDC} and non-suppressive T_{tolDC} lines. The clusters with a naïve-like phenotype (CD45RA$^+$CCR7$^+$) were explicitly present in the T_{tolDC} lines.

Suppressive capacity of T_{tolDC} and T_{mDC} subpopulations

To evaluate which of the three groups of cells in the T_{tolDC} lines defined by the multidimensional phenotypic analyses contains T cells with suppressive capacity, cells from T_{tolDC} and T_{mDC} lines were sorted based on the expression of CD45RA and CD25 and tested in a suppression assay (Figure 5). The CD45RA$^+$ T cells (representing group A) were only present in the suppressive T_{tolDC} line but lacked suppressive capacity. In contrast, both CD45RA$^-$CD25^{hi} and CD45RA$^-$CD25^{lo} T cells (representing group C and B, respectively) sorted from T_{tolDC} lines showed suppressive capacity (Figure 5B and 5C; one-way ANOVA p=0.03 and p=0.04), whereas CD45RA$^-$CD25^{hi} and CD45RA$^-$CD25^{lo} T cells derived from T_{mDC} did not suppress allogeneic CD4$^+$ T cell proliferation (Figure 5B and 5C).

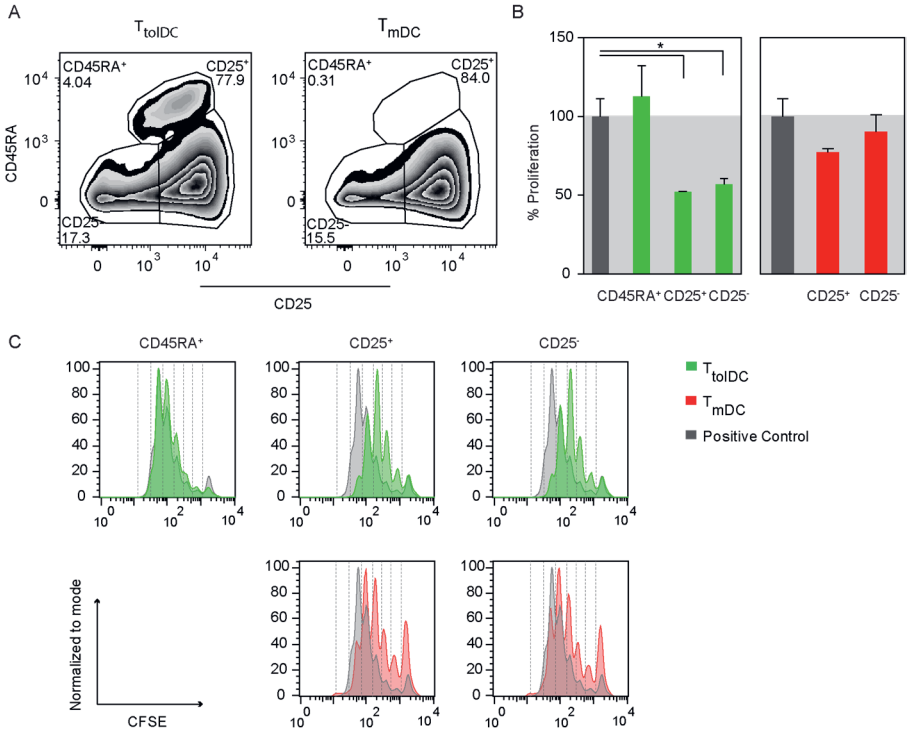

Figure 5. T$_{tolDC}$ with antigen experienced phenotype suppress naïve T cell proliferation. mDCs pulsed with proinsulin C19-A3 were co-cultured T$_{tolDC}$ or T$_{mDC}$ in a 1:10 ratio. Thereafter, T cells were stained and sorted based on CD45RA and CD25 expression. The suppressive capacity of the sorted populations was assessed in a suppression assay. A) Gating strategy of the cell sorting. B and C) Graphs and histograms depict proliferation of the CFSE-labelled allogeneic responder T cells in the presence of sorted T$_{tolDC}$ (green) or sorted T$_{mDC}$ (red) subsets relative to the responder proliferation alone (grey). Sorted memory-like CD25^{hi} and CD25^{lo}, but not naïve-like CD45RA$^+$ cells from T$_{tolDC}$ lines suppressed naïve T cell proliferation (one-way ANOVA p=0.03 and p=0.04). In contrast, sorted T$_{mDC}$ were not suppressive, irrespective of CD25 expression. Graphs depict representative of 2 independent experiments using T cell lines from different donors with similar results.

Next, we evaluated whether T$_{tolDC}$ can inhibit target-cell killing by autoreactive CD8$^+$ T cells. For this, clonal preproinsulin (PPI)-specific CD8$^+$ T cells were incubated with PPI-peptide pulsed target cells in the presence of total or sorted T$_{tolDC}$ populations. From the sorted T$_{tolDC}$ subpopulations, memory CD45RA$^-$CD25^{hi} T$_{tolDC}$ were most capable of inhibiting CD8$^+$ T cell-induced killing (figure 6A; two-way ANOVA p=0,017 and p=0,0058), while inhibition by CD45RA$^+$ and CD45RA$^-$CD25^{lo} T$_{tolDC}$ was insignificant compared to the total T$_{tolDC}$. The inhibiting capacity of the unsorted T$_{tolDC}$ line was likely

limited, since the inhibiting CD45RA$^-$CD25^{hi} subset represents a small proportion of the total T_{tolDC} (approximately 7%).

To further characterize the T_{tolDC} subpopulations, activation-induced Foxp3 expression was determined upon stimulation with proinsulin pulsed mDC. CD45RA$^-$CD25^{hi} and CD45RA$^-$CD25^{lo} T_{tolDC} showed high or intermediate expression of intracellular Foxp3, respectively, while CD45RA$^+$ T_{tolDC} did not express Foxp3. Lastly, cytokines were measured in the supernatant of T_{tolDC} subpopulations after re-challenge with proinsulin-pulsed mDC. Minor amounts of cytokines were detected in the supernatant of total T_{tolDC} (Figure 6C), corresponding with the data from unsorted T_{tolDC} lines (Figure 1C). The majority of cytokines produced by T_{tolDC} was derived from the CD45RA$^-$CD25^{hi} and CD45RA$^-$CD25^{lo} populations, while cytokine production by CD45RA$^+$ T_{tolDC} was nearly undetectable.

From this, we conclude that CD45RA$^+$ T_{tolDC} are non-activated, Foxp3-negative T cells, while T_{tolDC} with CD45RA$^-$CD25^{hi} and CD45RA$^-$CD25^{lo} phenotypes contain activated T cells with regulating capacity.

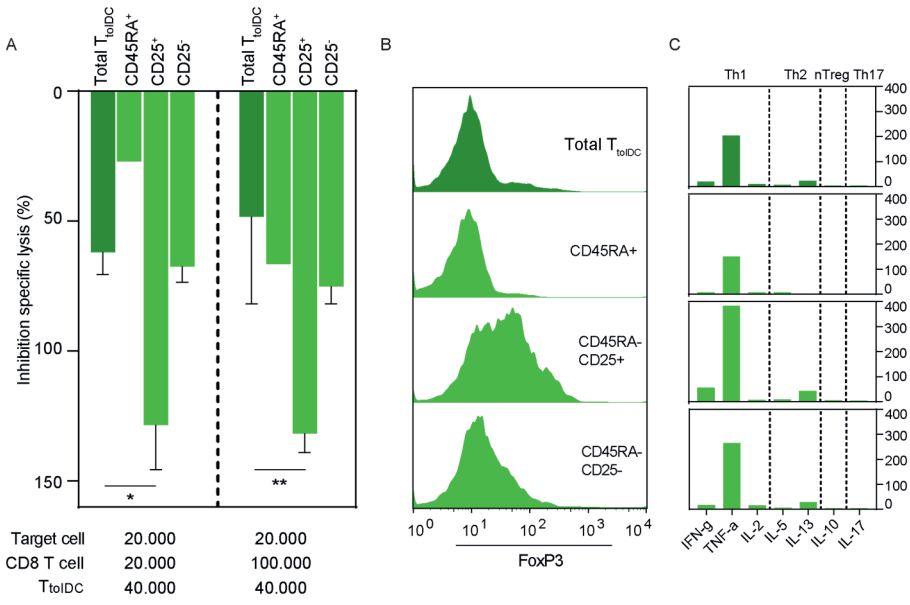

Figure 6. Memory-like T_{tolDC} expressing $CD25^{hi}$ protect target cells from CD8-induced killing. T_{tolDC} were stimulated overnight with proinsulin pulsed mDC. Thereafter, TtolDC cells were sorted into 3 groups based on the expression of CD45RA and CD25 ($CD45RA^+$, $CD45RA^-CD25^{lo}$ and $CD45RA^-CD25^{hi}$). A) The ability to inhibit $CD8^+$ T cell-induced killing was tested using PPI-specific $CD8^+$ T cell clone as effector and B cells loaded with PPI-peptide as target. Total T_{tolDC} or sorted subsets were incubated with CFSE-labelled target cells in a 2:1 ratio overnight. PPI-specific $CD8^+$ T cells were added for 4 hours, after which target cell counts were measured and % specific cell lysis was calculated. Specific lysis in the condition without T_{tolDC} were approximately 10% and 20% respectively and were set to the maximum (0% inhibition). Data are shown as mean % inhibition ± SD. From the T_{tolDC} subpopulations, $CD45RA^-CD25^{hi}$ T_{tolDC} shows significant inhibition of $CD8^+$ T cell induced killing compared to the unsorted T_{tolDC} (two-way ANOVA; p=0,017 and p=0,0058). B) Intracellular Foxp3 expression of T_{tolDC} line and the sorted T cell populations after overnight stimulation with proinsulin peptide-pulsed mDC. C) Cytokine production by total and sorted T_{tolDC} after overnight stimulation with proinsulin peptide-pulsed mDC.

Discussion

In this study, we extensively characterized the surface phenotypes and function of T cells stimulated with proinsulin peptide-pulsed tolDCs. Non-suppressive T cells were generated by tolDCs with an aberrant phenotype, underscoring the critical importance of CD52 and CD86 expression as quality control markers for tolDCs' ability to induce suppressive Tregs (29). Combining high-dimensional phenotyping with functional assays, we discovered that the presence of unresponsive, Foxp3 negative T cells holding a naïve-like phenotype ($CD45RA^{+}CCR7^{+}$) characterized suppressive T cell cultures induced by tolDCs. The functional suppressive T cells in tolDC-stimulated cultures lost CD45RA and obtained either $CCR7^{+}CD25^{lo}$ central memory or $CCR7^{-}CD25^{hi}$ effector memory phenotypes. Both subsets were capable of suppressing allogeneic $CD4^{+}$ T cell proliferation, while the inhibition of $CD8^{+}$ T cell killing was unique for effector memory $CD45RA^{-}CD25^{hi}$ T_{tolDC}. Contrary to IL-10-induced Tr1 (17, 18), suppressive T_{tolDC} did not produce anti-inflammatory cytokines, supporting our earlier observation on strongly suppressive Treg clones (22), while blocking of IL-10 and TGF-b did not affect the suppressive activity of tolDC-induced Tregs (8).

We propose that the naïve T cell population in T_{tolDC} lines reflects their arrest in activation and differentiation secondary to the concomitant induction of regulatory T cells. RNAseq analyses revealed several genes upregulated in tolDCs that are associated with inhibition of cell activation (29). Indeed, yields of T_{tolDC} after two weeks of culture rarely exceeded the number of plated naïve T cells at the start of the culture. In addition, T cell cultures stimulated by tolDCs never formed cell-clusters and retained the round morphology of inactive T cells (data not shown), possibly reflecting specific gene expression modifying the tolDC capacity to interact with cells and extracellular matrix (29). Which inhibitory molecules on tolDC or soluble mediators determine the lack of close contact with T cells including the underlying mechanisms remain to be investigated.

The mechanisms by which tolDC-induced Tregs modulate immune responses *in vivo* can be diverse. Islet infiltrating lymphocytes rarely contain Tregs in human T1D (31, 32). Instead, Tregs could protect beta cells (lacking HLA class II) indirectly by modifying antigen specific cells (APC) presenting proinsulin peptide in pancreas draining lymph nodes which in turn inhibit effector T cells and protect pancreatic beta cells (8). Tregs may also induce bystander suppression of neighbouring T cells by scavenging for essential cytokines and nutrients. Indeed, effector memory T_{tolDC} in this study showed low IL-2 content in the supernatant and inhibited islet autoreactive $CD8^+$ T cells, while expressing more Foxp3 than central memory T_{tolDC}. This difference could be explained by high expression of IL-2Rα (CD25), enabling this subset to capture and deprive other cells from IL-2, a mechanism proven essential to limit $CD8^+$ T cell activation but not to control $CD4^+$ T cell responses (33). In addition, the signalling by the captured IL-2 could support higher Foxp3 expression in this subset (34).

Using mass cytometry based analysis, the memory T_{tolDC} populations were further subdivided into clusters characterised by expression of previously described Treg markers such as HLA-DR (35), CD39 (36), Lag-3 (37), CTLA4 (38), ICOS (39), CCR4 (40) and CD161 (41, 42). T_{tolDC} with an effector memory phenotype co-expressed the markers CD28, CD38, CD39, CCR4, HLA-DR, ICOS and PD-1. In our analysis, we found a distinct population enriched in the T_{tolDC} lines co-expressing Lag-3, CTLA4 and GITR within the central memory and naïve phenotype. In addition, a small population characterized by CD161 was found within the T_{EMRA} phenotype suggesting that T cells with T_{EMRA} phenotype contain adaptive Tregs. This concurs with reports suggesting that T_{EMRA} are not merely unresponsive, exhausted cells (43). In view of their low frequency however, it is unlikely that only $CD161^+$ cells contribute to the suppressive activity of the $CD25^{hi}$ subset. Based on our findings here and our previous work (8), we presume that different T cell subsets such as $CD161^+$ and Lag-3^+ T cells contribute to the suppressive capacity of tolDC-induced Tregs.

The complexity and diversity of circulating nTregs has been described using mass cytometry and resembles the phenotypical signature that we report here on the tolDC-stimulated T cell lines, as well as those we reported previously (21, 22). nTregs, too, can be subdivided into several populations expressing CD45RO, CCR4, HLA-DR, ICOS, CD38, CD39 and a distinct $CD161^{+}$ population. Although this would suggest that induced antigen-specific Tregs look similar to $Foxp3^{+}$ nTregs, our studies show that most of these markers can also be present on activated non-suppressive T cells. Furthermore, we demonstrated that tolDCs also induce antigen-specific Tregs with $CD25^{lo}$ and $Foxp3^{dim}$ phenotype. Additional markers are therefore needed to identify induced suppressive cells in peripheral blood following immune modifying therapies. Subpopulations with unique suppressive qualities were identified, prompting follow-up analyses using an extended list of suppression-associated surface and intracellular molecules. The regulatory phenotypes described here may provide viable biomarkers of immune regulation in the clinic, enabling detection of induced Tregs after tolDC administration *in vivo*.

Conclusions

In summary, multiparameter analysis revealed phenotypical signatures of tolDC-stimulated T cells and showed that tolDC-induced Tregs obtain differential phenotypes, which corresponds to earlier findings of Treg diversity. We additionally demonstrate that partial tolerogenic modulation of DCs reflects in an atypical tolDC phenotype and reduced the Treg-inducing capacity. Suppressive T cells induced by tolDCs acquire different memory phenotypes, including cells expressing Lag-3, CD161 and ICOS. These markers, however, are also expressed by non-suppressive T cells. TolDC-induced T cell lines also retain or fix naïve-like T cells in a non-activated and non-suppressive state. This, however, mirrors the induction of suppressive activity. Our combined findings *in vitro* provide a basis for monitoring and optimization of the clinical use of tolDC therapies.

Acknowledgements

We thank Guillaume Beyrend for help with the data analysis and programming in R.

Authorship contributions

JSS, SL, KV, AJ and TN carried out the experiments. JSS, SL and TN performed the data analysis with support of VvU. VvU, BPFL and TH developed software for the data analysis and contributed to the study design. JSS, SL, TN, JJZ and BOR wrote the manuscript. BOR conceived the project and secured funding for this study.

Funding

This work was supported by the Wanek Family Project for Type 1 Diabetes, the Dutch Diabetes Research Foundation (grant number 31187) and the Dutch Arthritis Foundation (grant number 30514).

References

1. Gitelman SE, Bluestone JA. Regulatory T cell therapy for type 1 diabetes: May the force be with you. Journal of autoimmunity. 2016;71:78-87.
2. Marek-Trzonkowska N, Mysliwiec M, Dobyszuk A, Grabowska M, Techmanska I, Juscinska J, et al. Administration of CD4+CD25highCD127- regulatory T cells preserves beta-cell function in type 1 diabetes in children. Diabetes Care. 2012;35(9):1817-20.
3. Putnam AL, Brusko TM, Lee MR, Liu W, Szot GL, Ghosh T, et al. Expansion of human regulatory T-cells from patients with type 1 diabetes. Diabetes. 2009;58(3):652-62.
4. Todd JA, Evangelou M, Cutler AJ, Pekalski ML, Walker NM, Stevens HE, et al. Regulatory T Cell Responses in Participants with Type 1 Diabetes after a Single Dose of Interleukin-2: A Non-Randomised, Open Label, Adaptive Dose-Finding Trial. PLoS medicine. 2016;13(10):e1002139.
5. Alhadj Ali M, Liu YF, Arif S, Tatovic D, Shariff H, Gibson VB, et al. Metabolic and immune effects of immunotherapy with proinsulin peptide in human new-onset type 1 diabetes. Science translational medicine. 2017;9(402).
6. Ferreira GB, Kleijwegt FS, Waelkens E, Lage K, Nikolic T, Hansen DA, et al. Differential protein pathways in 1,25-dihydroxyvitamin d(3) and dexamethasone modulated tolerogenic human dendritic cells. Journal of proteome research. 2012;11(2):941-71.
7. Kleijwegt FS, Roep BO. Infectious tolerance as candidate therapy for type 1 diabetes: transfer of immunoregulatory properties from human regulatory T cells to other T cells and proinflammatory dendritic cells. Critical reviews in immunology. 2013;33(5):415-34.
8. Kleijwegt FS, Laban S, Duinkerken G, Joosten AM, Koeleman BP, Nikolic T, et al. Transfer of regulatory properties from tolerogenic to proinflammatory dendritic cells via induced autoreactive regulatory T cells. Journal of immunology (Baltimore, Md : 1950). 2011;187(12):6357-64.
9. Unger WW, Laban S, Kleijwegt FS, van der Slik AR, Roep BO. Induction of Treg by monocyte-derived DC modulated by vitamin D3 or dexamethasone: differential role for PD-L1. European journal of immunology. 2009;39(11):3147-59.
10. Kleijwegt FS, Jansen DT, Teeler J, Joosten AM, Laban S, Nikolic T, et al. Tolerogenic dendritic cells impede priming of naive CD8(+) T cells and deplete memory CD8(+) T cells. European journal of immunology. 2013;43(1):85-92.
11. Suwandi JS, Nikolic T, Roep BO. Translating Mechanism of Regulatory Action of Tolerogenic Dendritic Cells to Monitoring Endpoints in Clinical Trials. Front Immunol. 2017;8:1598.
12. Roep BO, Kleijwegt FS, van Halteren AG, Bonato V, Boggi U, Vendrame F, et al. Islet inflammation and CXCL10 in recent-onset type 1 diabetes. Clinical and experimental immunology. 2010;159(3):338-43.
13. Gibson VB, Nikolic T, Pearce VQ, Demengeot J, Roep BO, Peakman M. Proinsulin multi-peptide immunotherapy induces antigen-specific regulatory T cells and limits autoimmunity in a humanized model. Clinical and experimental immunology. 2015;182(3):251-60.
14. Hori S, Nomura T, Sakaguchi S. Control of regulatory T cell development by the transcription factor Foxp3. Science. 2003;299(5609):1057-61.
15. Bennett CL, Christie J, Ramsdell F, Brunkow ME, Ferguson PJ, Whitesell L, et al. The immune dysregulation, polyendocrinopathy, enteropathy, X-linked syndrome (IPEX) is caused by mutations of FOXP3. Nat Genet. 2001;27(1):20-1.
16. van der Vliet HJ, Nieuwenhuis EE. IPEX as a result of mutations in FOXP3. Clin Dev Immunol. 2007;2007:89017.
17. Roncarolo MG, Bacchetta R, Bordignon C, Narula S, Levings MK. Type 1 T regulatory cells. Immunological reviews. 2001;182:68-79.
18. Roncarolo MG, Gregori S, Battaglia M, Bacchetta R, Fleischhauer K, Levings MK. Interleukin-10-secreting type 1 regulatory T cells in rodents and humans. Immunological reviews. 2006;212:28-50.
19. Allan SE, Crome SQ, Crellin NK, Passerini L, Steiner TS, Bacchetta R, et al. Activation-induced FOXP3 in human T effector cells does not suppress proliferation or cytokine production. International immunology. 2007;19(4):345-54.
20. Kmieciak M, Gowda M, Graham L, Godder K, Bear HD, Marincola FM, et al. Human T cells express CD25 and Foxp3 upon activation and exhibit effector/memory phenotypes without any regulatory/suppressor function. J Transl Med. 2009;7.

21. Mason GM, Lowe K, Melchiotti R, Ellis R, de Rinaldis E, Peakman M, et al. Phenotypic Complexity of the Human Regulatory T Cell Compartment Revealed by Mass Cytometry. Journal of immunology (Baltimore, Md : 1950). 2015;195(5):2030-7.
22. Beringer DX, Kleijwegt FS, Wiede F, van der Slik AR, Loh KL, Petersen J, et al. T cell receptor reversed polarity recognition of a self-antigen major histocompatibility complex. Nature immunology. 2015;16(11):1153-61.
23. Hollt T, Pezzotti N, van Unen V, Koning F, Eisemann E, Lelieveldt B, et al. Cytosplore: Interactive Immune Cell Phenotyping for Large Single-Cell Datasets. Comput Graph Forum. 2016;35(3):171-80.
24. Pezzotti N, Hollt T, Lelieveldt B, Eisemann E, Vilanova A. Hierarchical Stochastic Neighbor Embedding. Comput Graph Forum. 2016;35(3):21-30.
25. van Unen V, Hollt T, Pezzotti N, Li N, Reinders MJT, Eisemann E, et al. Visual analysis of mass cytometry data by hierarchical stochastic neighbour embedding reveals rare cell types. Nat Commun. 2017;8.
26. Laban S, Suwandi JS, van Unen V, Pool J, Wesselius J, Hollt T, et al. Heterogeneity of circulating CD8 T-cells specific to islet, neo-antigen and virus in patients with type 1 diabetes mellitus. PLoS One. 2018;13(8):e0200818.
27. Kotecha N, Krutzik PO, Irish JM. Web-based analysis and publication of flow cytometry experiments. Current protocols in cytometry. 2010;Chapter 10:Unit10 7.
28. Kleijwegt FS, Laban S, Duinkerken G, Joosten AM, Zaldumbide A, Nikolic T, et al. Critical role for TNF in the induction of human antigen-specific regulatory T cells by tolerogenic dendritic cells. Journal of immunology (Baltimore, Md : 1950). 2010;185(3):1412-8.
29. Nikolic T, Woittiez NJC, van der Slik A, Laban S, Joosten A, Gysemans C, et al. Differential transcriptome of tolerogenic versus inflammatory dendritic cells points to modulated T1D genetic risk and enriched immune regulation. Genes Immun. 2017;18(3):176-83.
30. Zaki MJ. SPADE: An efficient algorithm for mining frequent sequences. Mach Learn. 2001;42(1-2):31-60.
31. Hull CM, Peakman M, Tree TIM. Regulatory T cell dysfunction in type 1 diabetes: what's broken and how can we fix it? Diabetologia. 2017;60(10):1839-50.
32. Willcox A, Richardson SJ, Bone AJ, Foulis AK, Morgan NG. Analysis of islet inflammation in human type 1 diabetes. Clinical and experimental immunology. 2009;155(2):173-81.
33. Chinen T, Kannan AK, Levine AG, Fan X, Klein U, Zheng Y, et al. An essential role for the IL-2 receptor in Treg cell function. Nature immunology. 2016;17(11):1322-33.
34. Zorn E, Nelson EA, Mohseni M, Porcheray F, Kim H, Litsa D, et al. IL-2 regulates FOXP3 expression in human CD4+CD25+ regulatory T cells through a STAT-dependent mechanism and induces the expansion of these cells in vivo. Blood. 2006;108(5):1571-9.
35. Baecher-Allan C, Wolf E, Hafler DA. MHC class II expression identifies functionally distinct human regulatory T cells. Journal of immunology (Baltimore, Md : 1950). 2006;176(8):4622-31.
36. Dwyer KM, Hanidziar D, Putheti P, Hill PA, Pommey S, McRae JL, et al. Expression of CD39 by human peripheral blood CD4+ CD25+ T cells denotes a regulatory memory phenotype. American journal of transplantation : official journal of the American Society of Transplantation and the American Society of Transplant Surgeons. 2010;10(11):2410-20.
37. Huang CT, Workman CJ, Flies D, Pan X, Marson AL, Zhou G, et al. Role of LAG-3 in regulatory T cells. Immunity. 2004;21(4):503-13.
38. Walker LS. Treg and CTLA-4: two intertwining pathways to immune tolerance. Journal of autoimmunity. 2013;45:49-57.
39. Ito T, Hanabuchi S, Wang YH, Park WR, Arima K, Bover L, et al. Two functional subsets of FOXP3+ regulatory T cells in human thymus and periphery. Immunity. 2008;28(6):870-80.
40. Sugiyama D, Nishikawa H, Maeda Y, Nishioka M, Tanemura A, Katayama I, et al. Anti-CCR4 mAb selectively depletes effector-type FoxP3+CD4+ regulatory T cells, evoking antitumor immune responses in humans. Proceedings of the National Academy of Sciences of the United States of America. 2013;110(44):17945-50.
41. Afzali B, Mitchell PJ, Edozie FC, Povoleri GA, Dowson SE, Demandt L, et al. CD161 expression characterizes a subpopulation of human regulatory T cells that produces IL-17 in a STAT3-dependent manner. European journal of immunology. 2013;43(8):2043-54.

42. Pesenacker AM, Bending D, Ursu S, Wu Q, Nistala K, Wedderburn LR. CD161 defines the subset of FoxP3+ T cells capable of producing proinflammatory cytokines. Blood. 2013;121(14):2647-58.
43. Faint JM, Annels NE, Curnow SJ, Shields P, Pilling D, Hislop AD, et al. Memory T cells constitute a subset of the human CD8+CD45RA+ pool with distinct phenotypic and migratory characteristics. Journal of immunology (Baltimore, Md : 1950). 2001;167(1):212-20.

Supplementary Figures

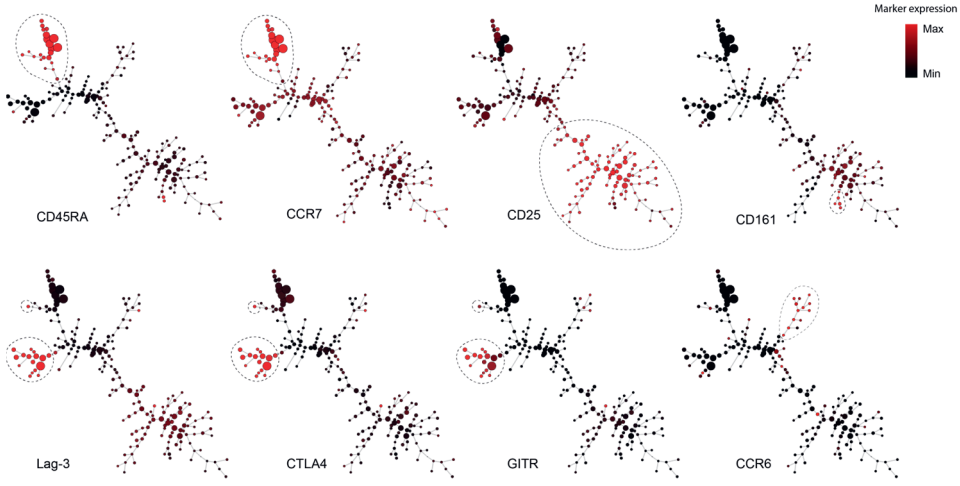

Supplementary figure 1. Marker expression of T_{tolDC} SPADE tree. The marker expression of CD45RA, CD45RO, CD25, CD161, Lag-3, CTLA-4 and GITR are visualised (representative T_{tolDC} sample 5).

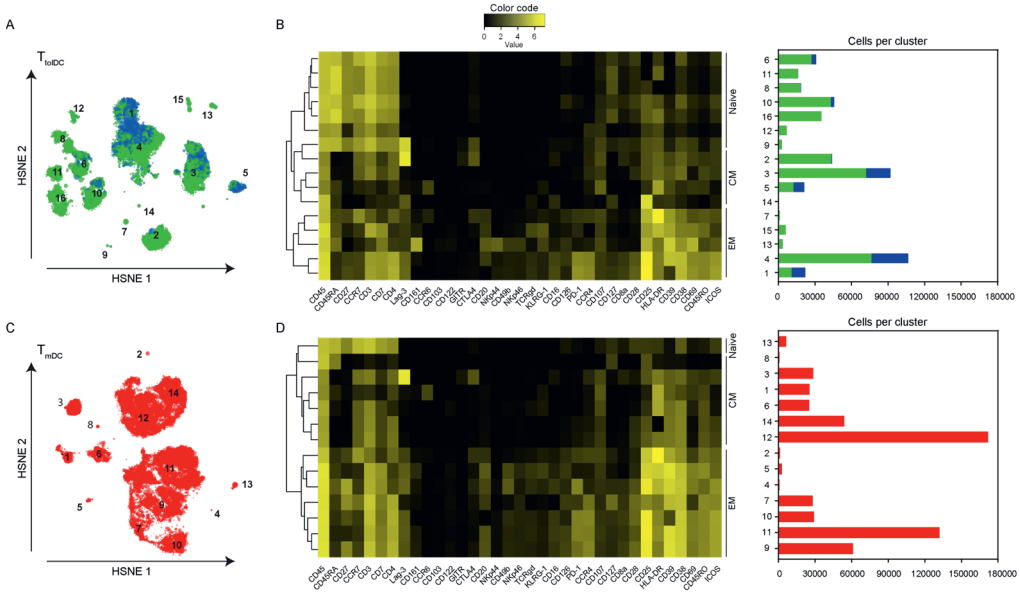

Supplementary figure 2. Marker expression signatures of T_{tolDC} and T_{mDC}. To visualise the individual marker expression of T_{tolDC} and T_{mDC} cells, lines were analysed separately in an HSNE. A) HSNE embedding of T_{tolDC} lines including cluster numbers (green: T_{tolDC}, blue: aberrant T_{tolDC} line 2). B) Heatmap of T_{tolDC} HSNE and abundancy histogram. C) HSNE embedding of T_{mDC} lines (red) and cluster numbers. D) Heatmap of T_{mDC} HSNE and abundancy histogram. Statistics of the abundancy heatmaps are shown in Supplementary table 1.

Supplementary table 1A. Statistics figure 4.

Cluster	T_{mDC}	T_{tolDC}	Non-suppressive T_{tolDC}
1	358	3013	115
A2	1575	3831	5
C3	780	597	115
C2	16030	778	174
C6	29972	12603	11792
C1	203439	73613	29316
B4	20836	2450	78
B6	2171	1338	204
B3	5007	1359	1550
B5	21164	11979	7294
B1	122366	33598	4825
B2	32206	5363	1455
B7	75850	32279	13260
C5	4927	10402	85
C4	22308	32080	394
A3	95	2230	7
A4	354	6896	71
A5	306	17673	59
A7	2967	45246	4420
A6	2938	76109	2016

Supplementary table 1B. Statistics supplementary figure 2.

Cluster	T_{tolDC}	Non-suppressive T_{tolDC}
6	27152	3682
11	15942	83
8	18341	142
10	43113	2456
16	35120	120
12	6544	117
9	2602	10
2	43435	543
3	72146	19711
5	12280	8659
14	352	12
7	890	153
15	5838	27
13	3144	124
4	76346	30243
1	10755	11170

Cluster	T_{mDC}
13	6340
8	826
3	28303
1	25231
6	25066
14	53813
12	171711
2	1153
5	2736
4	719
7	27997
10	29040
11	132026
9	61033